NuRD independent Mi-2 activity represses ectopic gene expression during neuronal maturation.

Gabriel N Aughey‡, Elhana Forsberg†, Krista Grimes†, Shen Zhang†, Tony D Southall*

†Equal contribution

*Correspondence to t.southall@imperial.ac.uk

Department of Life Sciences, Imperial College London, Sir Ernst Chain Building, London, UK

‡Current address: Department of Clinical and Experimental Epilepsy, UCL Queen Square Institute of Neurology, London, United Kingdom.

Abstract

During neuronal development, extensive changes to chromatin states occur to regulate lineage-specific gene expression. The molecular factors underlying the repression of non-neuronal genes in differentiated neurons are poorly characterised. The Mi2/NuRD complex is a multiprotein complex with nucleosome remodelling and histone deacetylase activity. Whilst NuRD has previously been implicated in the development of nervous system tissues the precise nature of the gene expression programmes that it coordinates are ill-defined. Furthermore, evidence from several species suggests that Mi-2 may be incorporated into multiple complexes that may not possess histone deacetylase activity. We show that Mi-2 activity is required for suppressing ectopic expression of germline genes in neurons independently of HDAC1/NuRD, whilst components of NuRD, including Mi-2, regulate neural gene expression to ensure proper development of the larval nervous system. We find that Mi-2 binding in the genome is dynamic during neuronal maturation and Mi-2 mediated repression of ectopic gene expression is restricted to the early stages of neuronal development, indicating that Mi-2/NuRD is required for establishing stable neuronal transcriptomes during the early stages of neuronal differentiation.

Keywords: NuRD, chromatin, differentiation, neurons, *Drosophila*

Introduction

Neuronal development involves the transition of multipotent precursor cells into highly specialised neurons with distinct morphological and biochemical characteristics. Extensive gene expression changes accompany the differentiation of precursors into specialised cell-types. These gene expression changes are underpinned by a dynamic chromatin environment in which regulation of nucleosome positioning and histone modifications ensures appropriate transcriptional responses. Whilst recent studies have provided illuminating descriptions of changes to chromatin accessibility and histone modifications during the process of neuronal differentiation (Aughey et al., 2018; Janssens et al., 2022; Preissl et al., 2018; Ziffra et al., 2021), the chromatin-interacting complexes that affect these changes are not well defined.

The Mi-2/NuRD complex is a multiprotein chromatin remodelling complex that influences gene expression via two separate enzymatic activities; ATP-dependent nucleosome remodelling, and histone deacetylation (Tong et al., 1998; Wade et al., 1998; Xue et al., 1998; Zhang et al., 1998). These activities are mediated by enzymes found in two distinct subunits. The nucleosome remodelling subunit, Mi-2, is a well conserved ATP-dependent nucleosome remodeller (CHD4 in mammals). While histone deacetylation is conferred by a separate HDAC (histone deacetylase) enzyme. NuRD components are widely conserved and broadly expressed in most metazoan tissues, reflecting the important role of the complex in gene regulation. NuRD has been reported to have critical roles in developmental processes, (e.g, in muscle (Gomez-Del Arco et al., 2016) and hematopoietic (Yoshida et al., 2008) cell differentiation), as well as regulation of pluripotent cell reprogramming (Rais et al., 2013).

Mi-2/NuRD complexes have critical roles in neurodevelopment and have been implicated in the aetiology of neurodevelopmental disorders (Hoffmann and Spengler, 2019). A recent study showed that Mi-2 is required in *Drosophila* neuronal lineages to deactivate notch responsive stem-cell enhancers in neuronal progeny, thereby ensuring the fidelity of differentiated cell fate in neurons (Zacharioudaki et al., 2019). Similarly, NuRD was shown to deactivate gene expression by acting on promoters of presynaptic genes to promote synaptic connectivity (Yamada et al., 2014). These studies suggest a predominantly suppressive role for NuRD in the regulation of gene expression. Whilst this is consistent with early models of NuRD activity as a repressive complex, more recent studies have presented a more nuanced role for NuRD in modulating gene expression, which may be neither activating or repressive, but acting to fine tune gene expression and reduce transcriptional noise (Bornelov et al., 2018; Burgold et al., 2019; Ragheb et al., 2020). Therefore, an important unanswered question is whether NuRD is primarily repressive in neuronal development, or whether it may facilitate control of active gene expression as demonstrated in stem cell models.

NuRD composition is dynamic in mouse cortical development, with alternate Mi-2/CHD paralogues incorporated to mediate distinct effects in different developmental stages (Nitarska et al., 2016). In *Drosophila* the components of the NuRD complex are well conserved, (although only single homologues of most NuRD proteins are identified). However, despite the strong conservation of NuRD constituent proteins, and ample evidence for physical interactions between them (Reddy et al., 2010; Zhang et al., 2016), the extent to which the canonical NuRD complex regulates gene expression in *Drosophila* is uncertain. A separate complex consisting of only Mi2 and MEP-1 (termed dMec), has been suggested to be more prevalent than NuRD in fly, and may be responsible for the majority of Mi-2 dependent phenotypes (Kunert et al., 2009). This observation has not been corroborated by further studies, however, NuRD-independent roles for Mi-2 may be present in human cells (Amaya et al., 2013). Alternatively, it is possible that since NuRD is comprised of pre-assembled modules (Zhang et al., 2016), and Mi-2 may exist as a peripheral component to the core complex (Low et al., 2016), the detection of non-NuRD associated Mi-2 may simply be a proteomic artefact that does not reflect a *bona fide* biological

activity. Therefore, the functional role of dMEC, and its relationship to the canonical NuRD holocomplex, remains poorly characterised.

Here, we set out to better understand the influence of Mi-2/NuRD on gene expression in the development of the central nervous system. Genomic profiling with Targeted DamID revealed distinct binding of Mi-2 containing complexes, NuRD and dMEC. Knockdown of Mi-2 in larval neurons resulted in ectopic expression non-neuronal genes as well as defective optic lobe development. Mi-2 represses lineage-inappropriate gene expression independently of NuRD, whilst optic lobe phenotypes are phenocopied by other members of the NuRD complex. We find that Mi-2 is not required for repression of non-neuronal genes after the early stages of differentiation, indicating that Mi-2 activity is critical for ensuring maintenance of the neuronal gene expression programme during maturation, but alternative mechanisms may be employed in fully differentiated neurons.

Results

Mi-2 is required in neurons for survival and larval locomotion.

Mi-2 has been shown to protect neural lineages from mitogenic notch signalling, indicating that NuRD has an important role in gene regulation in the neuroblasts and early progeny of *Drosophila* central nervous system (CNS) lineages. To better understand NuRD function in the fly CNS, we set out to examine the distribution of the core ATP-dependent nucleosome remodelling subunit Mi-2. We utilised a MiMIC insertion line in which Mi-2 is EGFP-tagged at its endogenous locus (*Mi-2-GFP* hereafter). We observed widespread Mi-2 expression with detectable EGFP signal in multiple cell-types in the third instar CNS (Figure 1A). EGFP signal was visible in nuclei of neural stem cells (NSCs) (as distinguished by their larger size and absence of Elav or Repo) as well as all neurons and some glia, (Figure 1A). The nuclear expression of Mi-2 in progenitor and post-mitotic cell-types in the larval CNS suggests that Mi-2 activity is likely to be involved in gene regulation in all stages of neuronal differentiation, including differentiated neurons.

To understand the importance of *Mi-2* expression in neurons, we used RNAi interference (RNAi) to induce cell-type specific knockdown of *Mi-2* in the CNS. An RNAi line targeting Mi-2 was previously shown to produce robust knockdown of Mi-2 in neuronal lineages, therefore, we decided to utilise this line for our study (Zacharioudaki et al., 2019). Using the pan-neuronal *elav*-GAL4 driver we observed lethality during late larval/pupal stages (Figure 1B). Whilst neuronal *Mi-2* appeared dispensable for embryogenesis and larval survival (possibly due to maternal contribution of Mi-2), we observed a severe mobility defect in larval crawling compared to controls (Figure 1C) indicating that *Mi-2* activity in neurons is required throughout development at all life-stages for normal neuronal function.

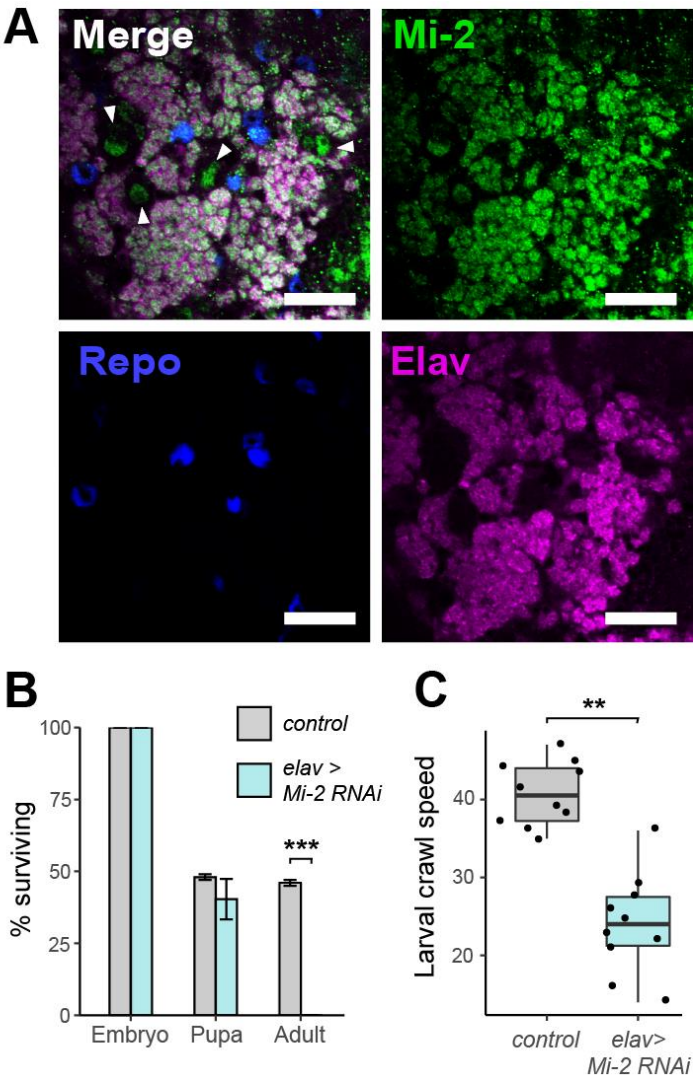

Figure 1. Critical role of *Mi-2* RNAi in *Drosophila* neurons. A) Third instar larval CNS of *Mi-2* GFP-trap line (scale bar = 20 µm). White arrows highlight NSC nuclei. B) Survival of *Mi-2* RNAi and control (*mCherry-RNAi*) flies during development (**** p < 0.001).* D) Larval crawl speed (cm/minute) in *Mi-2* RNAi and *mCherry* RNAi controls (** *p < 0.01*).

Mi-2 association with chromatin reveals the presence of distinct complexes

Our data, along with previous reports, suggest that Mi-2/NuRD has an essential role in the regulation of neuronal gene expression. However, it is unclear which genes Mi-2 regulates and whether its function is predominantly via NuRD or dMEC (Mi-2 and MEP-1 only). To better understand NuRD function in regulating neuronal gene expression, we profiled the genomic binding of NuRD complex components using Targeted DamID (TaDa) (Southall et al., 2013). This approach involves fusing a protein of interest to Dam methylase and expressing in a defined cell population, followed by enrichment and sequencing of selectively methylated regions which reflect loci at which the protein associates with DNA (reviewed in (Aughey et al., 2018).

116 We used Targeted DamID to profile genomic association of Mi-2 as well as NuRD components MTA1-
117 like and HDAC1 in neurons (defined by *elav*-GAL4 expression) in the larval CNS. MTA1-like is a core
118 component of the NuRD histone deacetylase subcomplex, with cells lacking MTA orthologues in
119 mammals considered to be effectively NuRD-null (Burgold et al., 2019), whilst HDAC1 is the histone
120 deacetylase subunit (also known as Rpd3). We also assayed for genomic binding of MEP-1, previously
121 reported to associate exclusively with Mi-2 as part of both the dMEC and NuRD complexes. Principal
122 component analysis revealed a single cluster including both Mi-2 and MEP-1 replicates, whilst the
123 remaining NuRD components, MTA1-like and HDAC1, appeared to be distinct (Figure 2A, B and C).
124 Similarity between Mi-2 and MEP-1 binding is further supported by the close correlation between the
125 two datasets (pearson R^2 = 0.94/0.95), which is almost as strong as that seen between replicates (Figure
126 EV1A). In contrast, both MTA-1like and HDAC1 showed relatively poor correlations to MEP-1 or Mi-2,
127 whereas their correlation with each other was slightly stronger. Whilst HDAC1 binding may be expected
128 to be poorly correlated with Mi-2 due to the inclusion of HDAC1 in protein complexes other than NuRD
129 (e.g. with Polycomb Group proteins (Tie et al., 2001)), the relatively low correlation with MTA1-like
130 points towards the possibility of distinct Mi-2 containing complexes having distinct binding in neurons.

131 To further understand the relationship between Mi-2 and other NuRD components at the chromatin
132 level, Mi-2 significantly bound peaks were compared to those of MEP-1, MTA1-like and HDAC1. We
133 found that the majority of MTA1-like peaks coincided with Mi-2, although a significant number of Mi-2
134 peaks did not overlap with MTA1-like (Figure 2C). We observed strong binding of HDAC1 throughout
135 the genome, however, a relatively low proportion of HDAC1 peaks intersected with Mi-2 peaks (Figure
136 2B, C), indicating that Mi-2 is found in association with chromatin without HDAC1 or MTA1-like at the
137 majority of loci.

138 We observed that around half of Mi-2 peaks coincided with either MTA1-like or HDAC1 with fewer still
139 having all three detected at the same site (around a quarter of total Mi-2 peaks). We also saw that a
140 smaller proportion of HDAC1 peaks were shared with Mi-2 compared to MTA1-like presumably due to
141 the inclusion of HDAC1 in other chromatin modifying complexes (Figure 2C). We also observed some
142 MTA1-like peaks that did not overlap with Mi-2 or HDAC1, suggesting that MTA1-like may have
143 undefined roles outside of NuRD. As previously indicated, MEP-1 and Mi-2 peaks intersected at almost
144 all loci. Inspection of the genomic features at which the various peaks were found to bind demonstrated
145 further disparity between Mi-2/MEP-1 and MTA1-like/HDAC1. We found that whilst HDAC1 was found
146 to be enriched at promoters and TSS, Mi-2 and MEP-1 were comparatively enriched in gene bodies,
147 particularly in exons (Figure 2D). Together these data suggest that multiple Mi-2 containing complexes
148 interact with chromatin in neurons, that may or may not possess histone deacetylase activity. In line
149 with previous reports, we refer to sites bound by Mi-2 and MEP-1 as "dMEC" hereafter (Kunert et al.,
150 2009), whilst sites with significant binding of all four profiled components are considered "NuRD" target
151 sites.

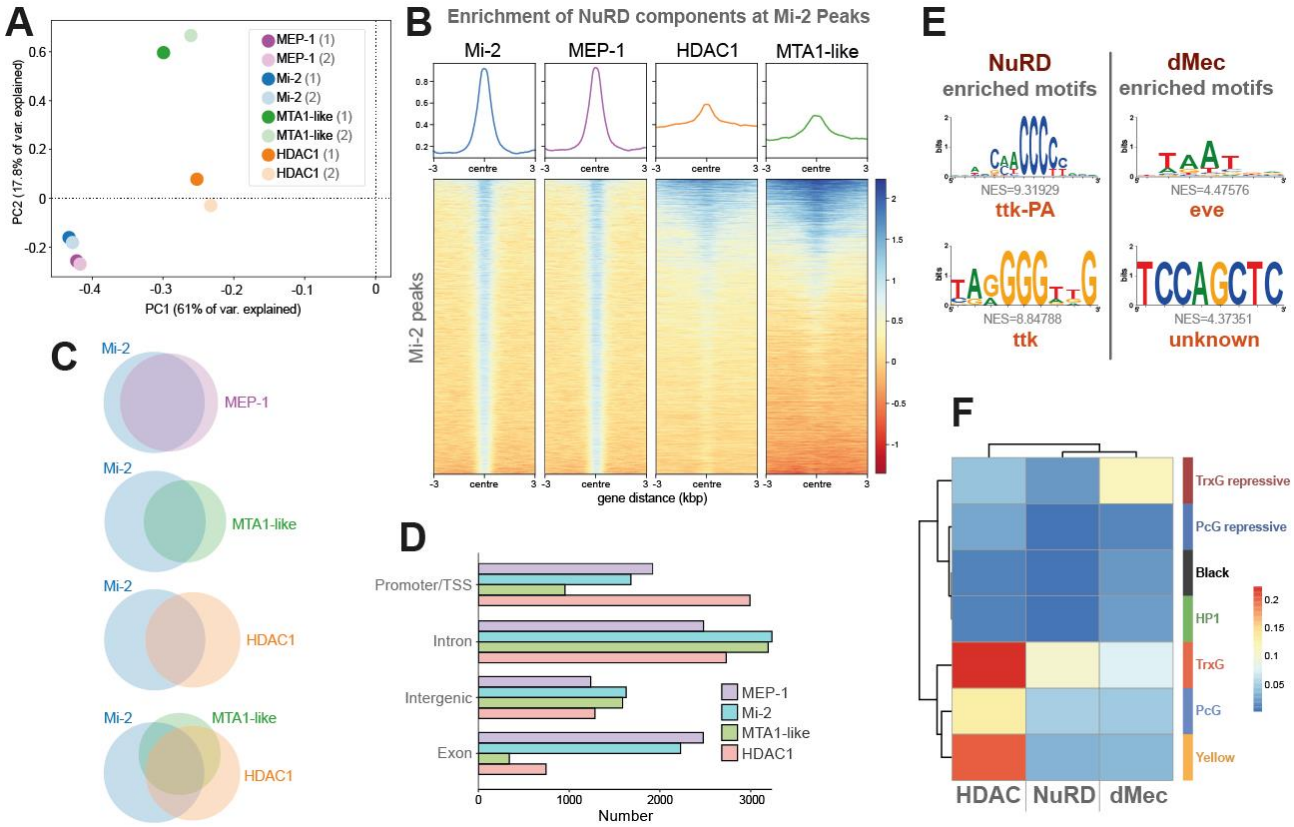

Figure 2. Genomic binding of NuRD components. A) Principal component analysis of all NuRD component binding in neurons including replicates. Mi-2/MEP-1 (blue/purple) cluster independently of MTA1-like (green) and HDAC1 (orange) reflecting greater similarity in their binding profiles. B) Heatmap and enrichment plots indicating binding at Mi-2 peaks. C) Venn diagrams indicating the number of overlapping peaks between NuRD subunits. All intersections between peaks occur at statistically significant frequencies (Fisher's exact test $p < 10^{-24}$). D) Peak annotation for Mi-2, MEP-1, MTA-1like and HDAC1 peaks. E) Top enriched motifs at NuRD and dMec peaks. F) Heatmap indicating jaccard similarity statistic between chromatin states and NuRD peaks (Mi-2, MEP-1, MTA-1like and HDAC1) and dMEC (Mi-2 and MEP-1 only), or HDAC1 peaks.

dMec and NuRD regulate different genes in neuronal differentiation.

Examining the gene ontology (GO) enrichment of genes bound by either NuRD or dMec revealed clear differences in the processes that were regulated by each complex. We found that NuRD-regulated genes were enriched for GO terms related to organismal development, with "nervous system development" amongst the top enriched terms (Figure EV1B). In contrast, genes with dMec peaks were enriched for terms relating to cilia function (Lattao et al., 2017) (Figure EV1C) (Appendix Figure S1) reflecting the prevalence of genes that are usually enriched in testis and not expressed in the CNS (although it should be noted that it is possible that some of these genes may also be expressed in fully differentiated sensory neurons). Terms relating to synaptic function were also enriched for genes bound by dMec, which may be expected of a group of genes the expression of which is regulated in neurons. However, inspection of

164 the genes comprising these categories reveals that many of these genes are expressed post-synaptically
165 outside the CNS (*GluRIIA, GluRIIC*) or in later stage pupal CNS in which neurons are in a more
166 differentiated state (e.g. *slo, Syt12*). These results are consistent with a model in which dMEC is largely
167 responsible for repression of gene expression, whilst NuRD is involved in coordinating appropriate
168 transcription of neuronal genes.

169 We examined NuRD and dMec bound sequences for enrichment of sequence motifs to see if we could
170 identify potential cofactors that may be involved in recruitment or regulation of these complexes. For
171 sequences bound by NuRD, we found that the most highly enriched sequence motifs corresponded well
172 to the consensus sequences for *tramtrack* (*ttk*) (Figure 2E). ttk has previously been shown to interact
173 with MEP-1 to recruit the NuRD complex (Reddy et al., 2010), and physical interactions with other NuRD
174 components have also been reported (Rhee et al., 2014). In contrast, the *ttk* motif was not enriched for
175 sequences covered by dMec peaks. Instead, the most highly enriched motif identified was a Hox-like
176 motif corresponding most closely to the transcriptional repressor *even-skipped* (*eve*). The differences in
177 the underlying sequences present at NuRD and non-NuRD Mi-2 binding sites suggest that these
178 complexes maybe recruited to target loci by distinct molecular factors.

179 To gain further insight into how Mi-2 containing complexes regulated gene expression we compared
180 binding to the state of the underlying chromatin. Chromatin can be grouped into discrete states
181 reflecting the occupancy of key regulatory proteins (Filion et al., 2010). We compared the binding of
182 HDAC1, Mi-2, MEP-1 and MTA1-like with published data describing chromatin state domains based on
183 a seven-state model (Marshall and Brand, 2017). We found that HDAC1 binding was associated with
184 broadly permissive chromatin states (Figure 2F). Whilst histone deacetylase activity has been thought
185 to be associated with repression of gene expression, these observations are consistent with previous
186 reports that have described enrichment of HDAC1 binding at active promoters (Wang et al., 2009).
187 Indeed, we also observe strong enrichment of HDAC1 binding at transcription start sites (TSS) as
188 previously reported (Figure EV1D). In contrast, Mi-2, MEP-1 and MTA1-like were found to be associated
189 with a mixture of permissive and repressive states, in particular with Trithorax-like permissive and
190 repressive states (Trx-G / Trx-G_repressive). Taking into consideration only regions that are bound by
191 either Mi-2/MEP-1 (dMec), HDAC1 alone, or all four proteins (i.e. NuRD), we saw that whilst NuRD
192 showed the greatest similarity to the Trithorax-like permissive state, Mi2/dMec more strongly
193 coincided with the transcriptionally silent Trithorax-associated repressive state, which is characterised
194 by the presence of Brahma as well as H1 linker histone. These observations support a model in which
195 NuRD independent Mi-2 binding largely mediates gene silencing/repression, whilst NuRD is involved in
196 the regulation of actively expressed genes.

197

198

199 ***Mi-2* knockdown results in misexpression of non-CNS genes.**

200 To determine the effect of Mi-2 loss on gene expression in neurons of the developing CNS, we performed
201 RNA-seq on larval CNS in which *Mi-2* had been knocked down in neurons by RNAi, and compared to
202 controls in which RNAi targeting mCherry was expressed using the same *elav*-GAL4 driver. We found
203 good correlation between replicates (Figure EV2A, B) and observed that the expression of *Mi-2* itself
204 was found to be significantly downregulated (Figure EV2C) in agreement with previous studies
205 (Zacharioudaki et al., 2019). We found that knockdown of *Mi-2* resulted in significantly more
206 upregulated genes than downregulated (397 downregulated vs 1467 upregulated) indicating that in the
207 context of developing neurons, *Mi-2* has a significant role in the repression of gene expression (Figure
208 3A-C). The top 30 upregulated and top 30 downregulated genes are shown in Figure EV2C, D.

209 Closer inspection of the top up-regulated genes revealed the presence of ectopically expressed genes
210 that are usually expressed in non-CNS tissues such as the germline. For example, *vasa* (*vas,* a well-
211 characterised ovarian germline marker) expression was (~3.5 log2 fold-change) increased compared to
212 controls (Figure 3B). Similarly, *gammaTub37C* – a female germline specific isoform of tubulin, was also
213 very highly upregulated (Figure EV2E), as well as *RpS5b*, encoding a germline specific ribosomal protein
214 (Figure EV2F). We also saw evidence of male-germline specific genes being upregulated, for example
215 *CG15446* (a transcription factor with testis specific expression) was expressed at much higher levels
216 than controls (Figure 3A). Comparison to tissue-specific transcriptomes indicates that the upregulated
217 genes are usually expressed outside the larval nervous system from a broad range of tissues, including
218 a large cluster of genes that have testis-enriched expression, as well as ovary, fat body, and digestive
219 system (Figure 3D and Appendix Figure S2A, B). Furthermore, Gene Ontology (GO) analysis of the
220 significantly up-regulated genes revealed enrichment of GO-terms that may be associated with neuronal
221 maturation or function, such as "ion transport", "sensory perception" and "cell projection assembly"
222 (Figure 3E). However, we also saw enrichment for unexpected terms such as "cilium assembly" that are
223 not typically associated with nervous system development or function.

224 We also observed misexpression of neuronal lineage specific genes that are not usually highly expressed
225 in the larval CNS but are expressed in specific neuronal populations in the adult nervous system. For
226 example, the antennal gene *a10* was seen to be very highly upregulated upon knockdown of *Mi-2* in the
227 larval CNS despite usually having expression restricted to the antennae in adult flies (Figure 3A and
228 Figure EV2C). Therefore, these data indicate that Mi-2 is required to ensure fidelity of neuronal
229 transcriptomes by suppressing expression of spatially and temporally inappropriate genes.

230

231

232

233

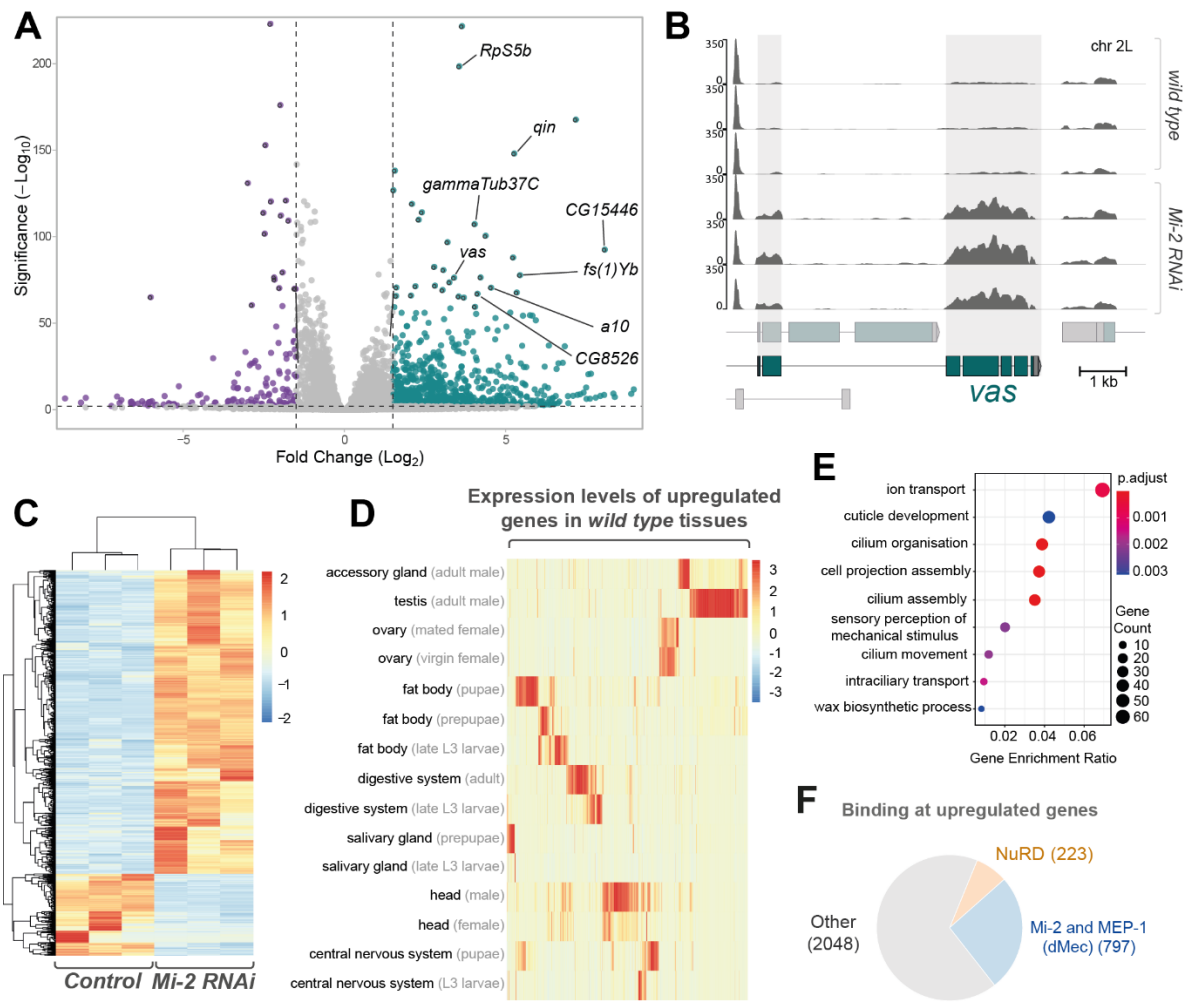

Figure 3. *Mi-2* knockdown in larval neurons results in extensive gene expression changes. A) Volcano plot showing significantly up-regulated (green) and down-regulated (purple) genes with fold-change. Selected mis-expressed genes are annotated. B) RNA-seq tracks showing *vas* mRNA expression in third instar larval CNS (Y-axis is RPKM). C) Heatmap showing relative changes in normalised read-counts between *Mi-2* RNAi and control replicates for all significantly differentially expressed genes (p-adj < 0.05, log2 fold change >1 or <-1). Significantly more genes are upregulated (1467) than downregulated (397). D) Enriched gene ontology terms for genes that are upregulated in *Mi-2* RNAi knockdown. E) Heatmap showing relative expression levels of upregulated genes across selected *Drosophila* tissues (full version in Appendix Figure S2).

Mi-2/dMEC represses ectopic gene expression independently of HDAC1

Having seen that Mi-2/NuRD components are distributed unequally in the genome, we examined how binding of NuRD components related to differentially upregulated genes. Since previous reports have suggested that dMec has a role in suppressing ectopic gene expression in cultured cells, we questioned whether this complex also plays a greater role in repressing ectopic gene expression in neurons. We found that NuRD binding (i.e. significant binding of Mi-2, MTA1-like, and HDAC1) was found at a much lower proportion of upregulated genes compared to those bound by dMec (Mi-2 and MEP-1) (223 and

242 797 genes respectively – (Figure 3F)). This observation led us to further investigate the role of dMec in
243 regulating gene expression compared to NuRD.

244 We used qPCR to confirm upregulation of a selection of highly mis-expressed candidate genes in *Mi-2*
245 knockdown flies (Figure 4A). Since RNAi mediated knockdowns have previously been associated with
246 off-target effects, we repeated these experiments with a second RNAi line which recapitulated the
247 upregulation of ectopic genes previously observed (Appendix figure S3). Since we saw distinct binding
248 of NuRD subunits, we first asked whether *HDAC1* was required for repression of ectopic genes. We found
249 that depletion of *HDAC1* by RNAi in neurons resulted in lethality during pupal stages similarly to *Mi-2*
250 (Appendix figure S4). However, *HDAC1* knockdown with two independent RNAi lines had no effect on
251 expression of any of the genes we tested that were upregulated upon *Mi-2* knockdown. Therefore, whilst
252 neuronal *HDAC1* is essential for survival, HDAC1 is not required for repression of some *Mi*-2 induced
253 ectopic gene expression in larval neurons (Figure 4A and Appendix figure S3).

254 We questioned whether the expression of ectopic genes in *Mi-2* knockdown was dependent on NuRD
255 (albeit without HDAC1 activity) or mediated by Mi-2 via NuRD-independent mechanisms. To address
256 this, we knocked down *MBD-like,* a core NuRD component thought to bridge the nucleosome
257 remodelling and histone deacetylation subunits. In *MBD-like* RNAi knockdown neurons, no difference in
258 gene expression of ectopic target genes was observed (Figure 4A), providing further evidence of *Mi-2*
259 acting independently of NuRD to mediate gene repression. Since MEP-1 binding in the genome appeared
260 to coincide with Mi-2 at almost every locus, we hypothesised that MEP-1 must also be part of the same
261 complex that confers repression of ectopic gene expression. Consistent with this idea, we saw that
262 knockdown of MEP-1 with *elav*-GAL4 was sufficient to cause upregulation of *vas* along with other target
263 genes tested (Figure 4A). Therefore, it appears that dMEC represses the expression of some genes in a
264 MEP-1 and Mi-2 dependent manner, without the requirement for HDAC1-mediated histone
265 deacetylation or other members of the NuRD complex.
266

267 **NuRD disruption in larval CNS causes severe optic lobe growth defects.**

268 Performing GO analysis for down-regulated genes from our Mi-2 knockdown RNA-seq indicated
269 enrichment of multiple terms related to cell division and stem cell function (Figure EV3A). This is
270 surprising since we knocked down *Mi-2* in neurons, which are exclusively post-mitotic and do not
271 express genes related to cell-division– therefore it is unlikely that Mi-2 could directly downregulate the
272 expression of these genes. To further understand the consequences of *Mi-2* depletion in neurons, we
273 examined dissected third instar larval CNS using confocal microscopy. We found that in *Mi-2* knockdown
274 resulted in severe optic lobe defects. Mi-2 knockdown brains were smaller, and it was evident that all
275 recognisable optic lobe structures (including inner and outer optic proliferation centres as well as
276 differentiating medulla and lamina neurons) were found to be completely absent (Figure 4B, C).
277 Interestingly, this included proliferative cells of the optic lobes and neuroepithelium (NE), including the

neuroblasts. We also examined *Mi-2* knockdown ventral nerve cords (VNCs) and observed no morphological changes or differences in NSC numbers (Figure EV3B, C). Therefore, we attributed the enrichment of GO terms relating to precursor cell function to the fact that a large number of cells expressing these genes were not present in the tissue from which RNA was extracted. Due to this severe phenotype, in which a large fraction of optic lobe cells are absent, we decided that we could not reliably identify genes that were downregulated as a consequence of Mi-2 loss rather than due to absence of cells expressing those genes. However, since we still saw far fewer downregulated than upregulated genes, this reinforces our conclusion that Mi-2 mainly acts to suppress gene expression in this context.

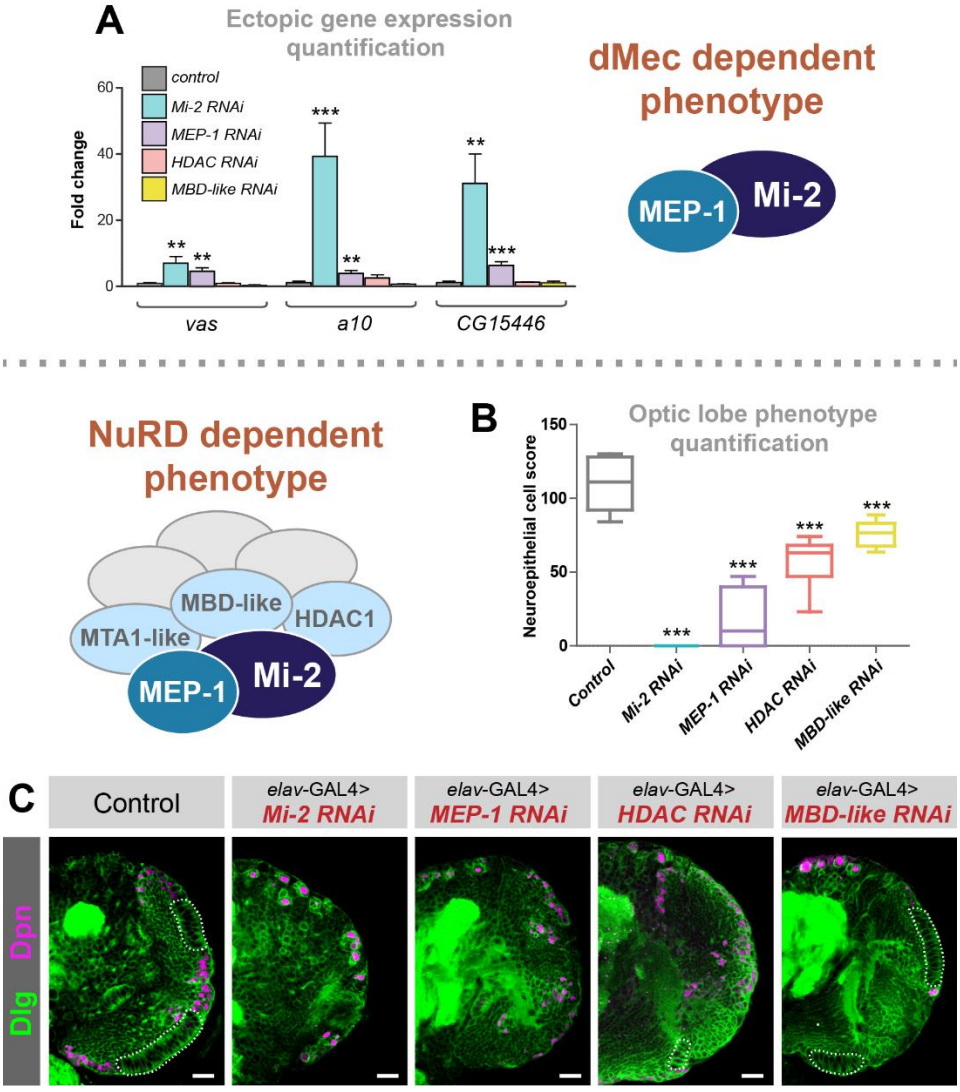

Figure 4. *dMec* knockdown causes ectopic gene expression and *NuRD* knockdown in neurons causes an optic lobe development phenotype.

A) Quantification of candidate gene expression (selected from upregulated genes in RNA-seq data) in knockdown genotypes (3 biological replicates for each group). ** *p < 0.01 and *** p < 0.001* (one-tailed student's t-test or Welch's t-test against control) Represented as mean ± SEM. B) Quantification of optic lobe neuroepithelial cells of genotypes shown in panel C (n >= 9 for each group). *** *p < 0.001* (one-tailed student's t-test or Welch's t-test against control). Represented as a box plot. C) Representative images of control (*elav*-GAL4*; ; mCherry*^{RNAi}), *Mi-2* knockdown, *MEP-1* knockdown, *HDAC1* knockdown and *MBD-like* knockdown in the third instar larval CNS (all scale bars = 20 µm).

287 Having seen NuRD-independent effects of *Mi-2* on gene expression, we questioned whether knockdown
288 of other NuRD complex components would phenocopy the optic lobe phenotype we observed when *Mi-*
289 *2 was* knocked down with *elav*-GAL4. In *MEP-1*, *HDAC1* and *MBD-like* knockdowns, the larval CNS
290 displayed a similar optic lobe defect to that of *Mi-2* (Figure 4B,C). Quantification of NE cells indicated
291 *that MEP-1*, *HDAC1* and *MBD-like* knockdowns had significantly fewer NE cells (Figure 4C), however the
292 phenotype was less severe with a small number being present in most brains (although this may be due
293 to less efficient RNAi mediated knockdowns in these lines). (Burgold et al., 2019) We also observed an
294 optic lobe phenotype with knockdown of *MTA-1* (Figure EV3D, E). Therefore, due to the similarity of
295 phenotypes observed with knockdowns of multiple NuRD complex members we concluded that whilst
296 *Mi-2* functions to repress some ectopic genes in a NuRD independent manner, its effect on optic lobe
297 development involves the activity of the NuRD holocomplex (although it remains unclear whether dMEC
298 also contributes to this phenotype). Conversely, the ectopic upregulation of genes is independent of
299 NuRD/histone deacetylation, and is not required to produce optic lobe developmental defects in the
300 larva (although since the phenotypes vary in severity, there may be some contribution of dMec induced
301 ectopic gene expression on NE survival).

302

303 **Fully differentiated neurons do not require Mi-2 for silencing of ectopic gene expression or**
304 **proper optic lobe development in larvae**

305 Factors involved in the maintenance of neuronal transcriptomes during early neuronal maturation can
306 have less severe phenotypes in fully differentiated neurons in which synapses have been formed
307 (Hassan et al., 2020; Southall et al., 2014). This correlates with observed changes to the underlying
308 chromatin landscape which is dynamic during differentiation and neuronal maturation (Aughey et al.,
309 2018; Marshall and Brand, 2017). Notch-induced hyperplasia in neuronal lineages is enhanced by the
310 knockdown of *Mi-2*, however, this effect is diminished as cells become more differentiated
311 (Zacharioudaki et al., 2019). In our previous knockdown experiments, we employed the *elav*-GAL4
312 driver to target all neurons in the *Drosophila* larval CNS. This includes a substantial proportion of
313 neurons that are post-mitotic cells, but not fully differentiated to the point at which synaptic proteins
314 are expressed. In fact, it has been suggested that the majority of larval brain *elav*-expressing neurons
315 contribute relatively little to neuronal function (Eichler et al., 2017), since they do not possess axons or
316 dendrites or express ion-channels associated with neurotransmission (Ravenscroft et al., 2020), despite
317 comprising a large proportion of the total cells in the larval brain (Jiao et al., 2021). Therefore, we
318 questioned whether Mi-2 dependent optic lobe phenotypes or de-repression of silenced genes would be
319 observed when Mi-2 was knocked down in either progenitor cells or fully differentiated neurons.

320 The larval CNS consists of mostly immature neurons that are produced post-embryonically. However,
321 there is a sizeable population of fully differentiated neurons that persist from the embryo that express
322 the mature neuron marker nSyb. The majority of these are found outside of the optic lobes in the central

323 brain and VNC, however there are a very small number of nSyb cells found in the optic lobe lamina (Jiao
324 et al., 2021). To rule out the contribution of signalling from these mature neurons being responsible for
325 the morphological phenotypes, we examined brains in which *Mi-2* RNAi was driven with *nSyb*-GAL4.
326 Knockdown of Mi-2 using nSyb-GAL4 did not result in any detectable change in *vas* mRNA levels (Figure
327 5A). We also tested whether depletion of Mi-2 in adult neurons was sufficient to de-repress *vas*
328 expression using a temperature sensitive GAL80 to de-repress *Mi-2* RNAi in neurons using *elav*-GAL4
329 for a 24-hour period after eclosing. As in third instar larvae, no change in *vas* expression was detectable
330 in adult heads (Figure EV4A). We also tested for expression of *a10* and *CG15446*, which also did not
331 show any increased expression in adult neurons, indicating that Mi-2 is only required for the repression
332 of ectopic gene expression in the early stages of neuronal development. We used *wor*-GAL4, to drive *Mi-*
333 *2* RNAi in NSCs (it should be noted that this driver is likely to also affect the newly born GMC and early
334 differentiating neurons due to perdurance (Johnson et al., 2018) (Figure 5B). Using *wor*-GAL4 to knock
335 down *Mi-2* in NSCs, we performed qPCR to detect changes in gene expression. When *Mi-2* was knocked
336 down in NSCs, the expression of female germline marker *vas* was significantly upregulated (Figure 5A),
337 as previously seen with *elav*-GAL4 knockdowns. *vas* expression was upregulated to a lower extent than
338 when induced with *elav*-GAL4 (~4 fold increase compared to ~10 fold), however this may be due to the
339 lower number of affected cells expressing *wor*-GAL4 rather than reflecting a difference in the
340 requirement for Mi-2 for repression of *vas* in NSCs. It should also be noted that it is possible that a small
341 amount of perdurance of GAL4 into NSC progeny may be responsible for de-repression of non-neuronal
342 target genes in immature neurons or GMCs, rather than due to an effect exclusively in NSCs.

343 Surprisingly, we found that *Mi-2* knockdown in NSCs showed no apparent defects in optic lobe
344 development, with brain lobes having a similar morphology and neuroepithelial cell numbers to
345 controls (Figure 5C and Figure EV4B, C). In contrast to when *Mi-2* was depleted in neurons (Figure 1D),
346 loss of *Mi-2* in NSCs did not result in larval locomotion defects (Figure EV4D). However, *Mi-2* knockdown
347 in NSCs did result in lethality, with 100% dying as pupae. Therefore, since brain size, morphology and
348 movement are normal in these animals, these results suggest that Mi-2 is not required for stem cell
349 division or differentiation into neurons. Nevertheless, Mi-2 function in NSCs is required for the correct
350 functioning of subsequently born neurons.

351 Having seen that expression of *Mi-2* RNAi in neuronal precursors was not responsible for the optic lobe
352 phenotype, we questioned whether other unexpected expression may be responsible. *elav*-GAL4 may
353 drive some expression in embryonic glial cells (Berger et al., 2007), therefore, we questioned whether
354 unexpected glial knockdown of *Mi-2* may have resulted in a disruption of signalling that maintains the
355 optic lobe stem cells. To address this, we repeated the *Mi-2* knockdown with an *elav*-GAL4 driver
356 combined with *repo*-GAL80, to repress unwanted expression of the RNAi hairpin in glia. In these
357 animals, we observed the same severe optic lobe phenotype as previously with *elav*-GAL4 alone (Figure
358 EV4E). These data indicate that *Mi-2* knockdown in neurons may affect optic lobe growth via a non-cell-
359 autonomous mechanism. This may be partly explained by the requirement for innervation by

360 photoreceptor neurons to initiate neurogenesis in the developing visual centres (Huang and Kunes,
361 1996; Selleck and Steller, 1991), which would be affected by *elav*-GAL4 knockdown of *Mi-2*. We also
362 examined 1st instar *Mi-2* knockdown brains and found that the typical rosette of NE cells is present
363 (Figure EV4F). Therefore, the NE is present at earlier stages of development, however, is not persisting
364 to later stages. As *elav*-GAL4 has never been reported to be expressed in NEs, the role of any glial
365 expression of *Mi-2* RNAi has been eliminated (Figure EV4E), and knockdown of *Mi-2* in neuroblasts has
366 no phenotype (Figure EV4B, C), this strongly suggests that there is a non-cell-autonomous mechanism
367 occurring. However, a full explanation of this phenotype is beyond the scope of this study and further
368 work must be conducted to determine the mechanism by which the optic lobe defect occurs.

369 In contrast to knockdown in all neurons including immature neurons with *elav*-GAL4, depletion of *Mi-2*
370 exclusively in mature neurons did not produce overt morphological phenotypes and no significant
371 difference in neuroepithelial cell numbers were detected when compared to controls (Figure 5C and
372 Figure EV5A, B). As with the other drivers used, *Mi-2* knockdown with *nSyb*-GAL4 resulted in 100 %
373 lethality during pupal stages. Therefore, whilst Mi-2 is required in mature neurons, the morphological
374 defects observed in the larvae do not arise from loss of Mi- 2 function in fully differentiated neurons in
375 the larval CNS.

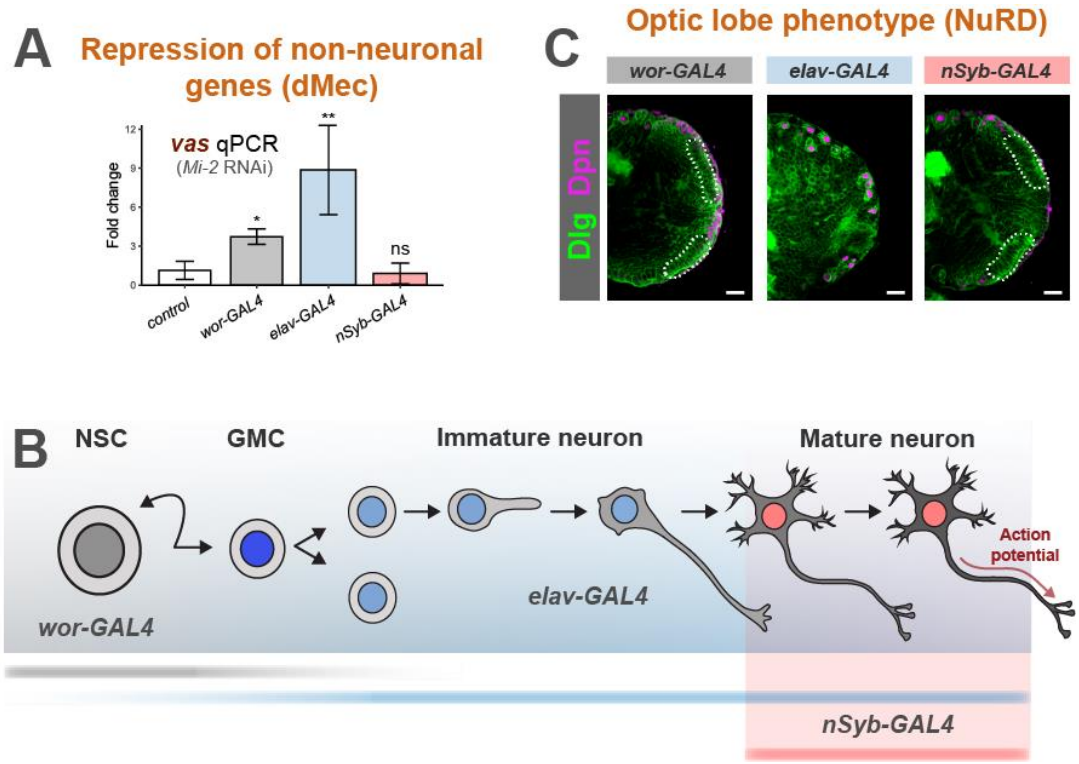

376

Figure 5. Differential requirements of Mi-2 during neuronal differentiation. A) Ectopic expression of *vas* when *Mi-2* is knocked down at different stages of differentiation. (3 biological replicates for each group). * $p < 0.05$ and ** $p < 0.01$ (one-tailed student's t-test against control) Represented as mean ± SEM. B) Representation of expression of GAL4 drivers used. C) Larval brain optic lobe morphology when *Mi-2* is knocked down at different stages of differentiation Elav = green, Dpn = magenta.

377 **Dynamic Mi-2 binding during neuronal differentiation**

378 We reasoned that varying consequences of *Mi-2* loss at different stages of neuronal differentiation may
379 be reflected by changes to Mi-2 binding in different cell types. To examine differences in Mi-2 genome
380 occupancy in precursor cells vs fully differentiated cells, we profiled Mi-2 (using TaDa) in two further
381 populations of cells in the larval brain. Firstly, in NSCs (*wor*-GAL4 - This driver has been used previously
382 to produce Targeted DamID profiles that are distinguishable from those produced from GMCs/newly
383 born neurons. However, it should be noted that due to perdurance of GAL4, these profiles likely
384 represent the early stages of neurogenesis more generally rather than specifically NSCs. We then also
385 profiled mature neurons (*nSyb*-GAL4) in the larval CNS, in which we saw no change in *vas* expression
386 upon *Mi-2* knockdown. Since these neurons do not reflect the direct descendants of those produced by
387 the *wor*-expressing NSCs in the larval brain (being mostly derived from earlier embryonic
388 neurogenesis), they may also display lineage specific changes in Mi-2 binding.

389 Binding profiles between cell types were compared and regions of differential binding identified (Figure
390 6 A,B). Total neurons (*elav*-GAL4) show the largest number of significantly bound peak regions (10,420),
391 with mature neurons binding 7054 genes (Figure 6B). However, the number of peaks common to each
392 cell type is relatively low. Therefore, Mi-2 binding is highly dynamic during neuronal differentiation. In
393 many individual genes, sites with enriched binding in NSCs showed a different set of enriched Mi-2
394 binding sites in immature neurons (Figure 6 A, C). A similar change occurs from immature to mature
395 neurons, with 2144 genes that contain both immature-vs-mature and mature-vs-immature regions of
396 Mi-2 enrichment (Figure 6C and the example of *chn* in Figure 6A).

397 Motif enrichment analysis of the differentially bound regions identified transcription factor binding sites
398 (Figure 6D). Binding sites for l(3)neo38, crol and ttk88 are present in the NSC-vs- immature comparison,
399 suggesting that these sites are occluded in NSCs but available for binding in neural progeny.
400 Interestingly, l(3)neo38 occupies a set of putative neuronal enhancers in the developing embryo and is
401 required for the proper formation of the larval brain (Reddington et al., 2020). l(3)neo38 and crol have
402 both been implicated in the regulation of heterochromatin silencing (Schneiderman, 2010 & Swenson,
403 2016). While ttk88 sites are enriched for binding in NSC-vs-immature neurons, ttk69 sites (a different
404 splice isoform) are enriched in the immature-vs- mature comparison. Finally, fd102C and Cf2 sites have
405 greater Mi-2 binding in mature-vs-immature neurons. Fd102C is an uncharacterised forkhead
406 transcription factor highly expressed in the developing and adult nervous system (Krause et al., 2022)
407 and Cf2 is a zinc-finger factor involved in follicle cell fate and myogenic gene expression (Bagni et al.,
408 2002; Hsu et al., 1996). These data indicate that a dynamic repertoire of transcription factors may direct
409 or be influenced by dynamic Mi-2/NuRD binding during neuronal maturation. It is clear from the broad
410 changes in binding that Mi-2 coordinates a distinct gene expression programme in early neuronal
411 lineages compared to fully differentiated neurons corresponding to the differences in phenotypic

outcomes observed (although some of the observed changes may be due to embryonic vs larval neuronal lineage differences).

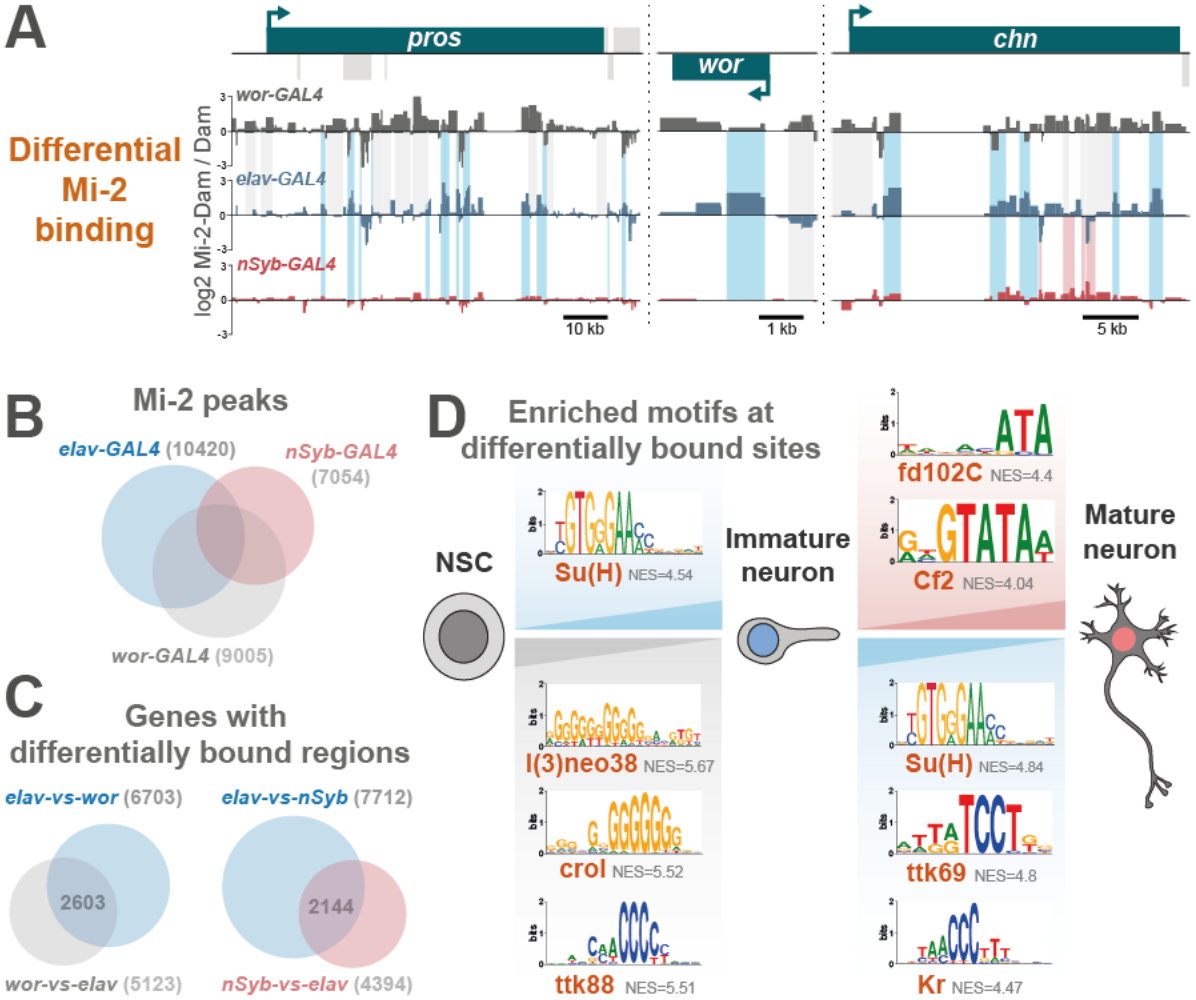

Figure 6. Dynamic Mi-2 binding during neuronal differentiation. A) Examples of differential genomic binding of Mi-2 at neural genes. B) Overlap of Mi-2 binding peaks in NSCs, immature neurons and mature neurons. C) Number and overlap of genes with differential Mi-2 binding. D) Motif analysis of differentially bound regions.

Su(H) (Notch co-factor) motifs were enriched in both immature-vs-NSC and immature-vs-mature regions (Figure 6D). This aligns with previous work showing that Mi-2 is required to deactivate notch responsive stem-cell enhancers in neuronal progeny (Zacharioudaki et al., 2019). Mi-2 was implicated in the silencing of genes in the *E(spl)-C* locus, with broad binding of Mi-2 across this locus having been demonstrated in *Drosophila* cell lines (Ho et al., 2014; Kreher et al., 2017). Consistent with this result we saw strong binding of Mi-2 across the *E(spl)-C* locus in both NSCs and immature neurons (Figure EV5C). This study also showed that in more mature neurons Mi-2 depletion was not sufficient to enhance notch-induced overgrowth. We saw no significant binding of Mi-2 in mature neurons across the entire region

424 (approx. 50 kb), supporting the conjecture that in more fully differentiated cells, continued chromatin
425 remodelling of the *E(spl)* genes by Mi-2 is not required for their repression.

426

427 Discussion

428 Our data provide evidence for Mi-2 activity in repressing ectopic gene expression independently of
429 NuRD. Mi-2 from *Drosophila* or humans is sufficient for the remodelling of nucleosomes *in vitro*, in the
430 absence of other NuRD components (Brehm et al., 2000; Wang and Zhang, 2001). In mouse embryos,
431 Mi-2 orthologue CHD4 was shown to be necessary for lineage specification in a manner that was
432 independent of MBD proteins that are required for a functional NuRD complex (O'Shaughnessy-Kirwan
433 et al., 2015). Similarly, loss of CHD4 in human erythroid cells resulted in de-repression of fetal *γ-globin*,
434 which occurred independently of NuRD (Amaya et al., 2013). Furthermore, similarly to what we observe
435 in neurons, MBD3 was found to bind at less than half of all CHD4 sites in mouse ESCs and were anti-
436 correlated to histone markers associated with transcription (Bornelov et al., 2018). Therefore, it is likely
437 that NuRD-independent Mi-2 regulation of gene expression is a conserved feature in animal cells.

438 A previous study concluded that Mi-2 in complex with MEP-1 (dMec) was the dominant Mi-2 containing
439 complex in *Drosophila* Kc cells (Kunert et al., 2009). From this observation it could be inferred that NuRD
440 plays a relatively minor role in the regulation of gene expression. However, this conclusion was drawn
441 based on biochemical interactions and relative stoichiometries of NuRD components. We find that in
442 contrast to the abundance of dMec, around a third of Mi-2 peaks intersect with MTA1-like, indicating
443 that NuRD is prevalent at a large number of loci. Furthermore, severe optic lobe phenotypes were
444 observed with multiple NuRD components, which did not always include de-repression of lineage-
445 inappropriate genes. These data indicate that despite being present at lower amounts than dMec, NuRD
446 plays a critical role in nervous system development. Whilst it is possible that the proportions of
447 NuRD/dMec may differ between the CNS and cultured cells, our data suggest that the relative amounts
448 of protein detected by biochemical means may not be reflective of either the distribution of sites at
449 which complexes are associated in the genome, or the severity of consequences resulting from their loss.
450 It is currently unclear whether an analogous complex to dMEC exists in mammals. MEP-1 does not share
451 direct orthology with any single mammalian transcription factors, however, since it is clear that CHD4
452 is capable of conferring NuRD-independent activities in mammalian cells, it is possible that there are
453 unidentified mammalian genes that act in an analogous role to MEP-1.

454 Our data indicates that Mi-2 represses non-neuronal genes such as those normally expressed in the
455 germline, and that this is largely independent of NuRD. Interestingly, Mi-2/dMec depletion resulted in
456 proneural gene expression in Kc cells (Kunert et al., 2009), suggesting that Mi-2 may repress ectopic
457 gene expression in multiple tissue types dependent on context. A similar phenotype has also been
458 reported in *C. elegans* in which MEP-1/Mi-2 knockdown resulted in expression of germline genes in

459 somatic tissues, indicating that this may be a conserved function of Mi-2 (Unhavaithaya et al., 2002). It
460 is possible that in mammals, NuRD-independent CHD4 function is also required for gene repression
461 since loss of CHD4 in lymphocytes results in upregulation of non-hematopoietic genes (Arends et al.,
462 2019). However, it remains unclear whether this transcriptional repression is dependent on histone
463 deacetylase activity/NuRD, or NuRD-independent CHD4 activity.

464 Mi-2 is only required to suppress ectopic gene expression up to the early stages of neuronal
465 development, whereas in more fully differentiated cells it is dispensable. Therefore, it is likely that other
466 molecular factors are required for the repression of these genes following synaptogenesis. Mi-2/dMEC
467 may be required to establish a stable epigenetic state following recruitment by sequence specific
468 transcription factor binding, after which these states are maintained by separate chromatin modifying
469 proteins or complexes. The degree of differential binding of Mi-2 observed during neuronal
470 differentiation is consistent with the idea that Mi-2 coordinates a distinct gene expression programme
471 during early neuronal differentiation compared to in mature neurons. The identification of different
472 transcription factor binding sites during development suggests that either the cognate transcription
473 factor is recruiting Mi-2 to these sites, or that Mi-2 is independently positioned there to establish a
474 chromatin state to prevent the binding of the factor. Since it seems that Mi-2 exhibits at least two
475 independent modes of interacting with chromatin (i.e. via dMEC/NuRD), either or both of these models
476 may be true depending on the presence of other subunits and wider genomic context. Su(H) binding
477 sites are found at sites enriched in immature neurons versus both NSCs and mature neurons (Figure
478 6D). Furthermore, l(3)neo38 binding sites, that have been identified at neural enhancers (Reddington
479 et al., 2020), are more strongly bound in NSCs compared to immature neurons. Therefore, for at least
480 Su(H) and l(3)neo38, Mi-2 appears to be blocking binding of these factors (loci specific) at stages of
481 differentiation where their function is not required/wanted.

482 Together, our data highlight that the activity of Mi-2 is dependent on both its molecular and
483 developmental context. These data highlight the importance of detailed analyses of individual subunits
484 in inferring functions of chromatin modifying complexes in complex multicellular tissues to fully
485 understand their role in gene regulation.

486

487 Materials and Methods

488 Fly stocks

489 Unless stated otherwise flies were kept on standard fly food media at 25 degrees. A full list of fly stocks
490 used in this study can be found in Appendix Table S1. Mixed sex larvae/flies were used for all
491 experiments.

492 Immunohistochemistry and imaging

493 Third instar larval CNS were dissected in PBS and fixed for 20 min with 4% formaldehyde in PBS. The
494 following antibodies were used in this study: rat anti-Elav (7E8A10 - Developmental Studies Hybridoma
495 Bank), chicken anti-GFP (600-901-215 - Thermo scientific), mouse anti-DLG (4F3 - Developmental
496 Studies Hybridoma Bank), and guinea pig anti-Dpn (kind gift from A. Brand). Samples were imaged using
497 a Zeiss LSM510 confocal microscope and images processed using LSM Image Browser and image J. To
498 quantify an OPC NE cell score for each genotype, 3rd instar larval brains were mounted dorsal side down
499 and full image stacks (2 µm intervals) of the brain lobe were taken using the DLG channel. The number
500 of OPC NE cells were counted at image slices at ¼, ½ and ¾ through the stack (identified by position
501 and morphology) and added together to give the score. To quantify the number of Dpn positive cells in
502 VNCs, , whole VNC image stacks were analysed using the 3D Objects Counter in Fiji (Bolte and
503 Cordelieres, 2006). For each genotype, a Shapiro–Wilks test was performed to calculate if the
504 experimental and control data had normal distributions. If they did, a one-tailed student's t-test was
505 applied, and if not a Welch's t-test was applied.

506 **Generation of Targeted DamID lines**

507 *MEP-1* and *Mi-2* were amplified by PCR from cDNA with primers including 30 bp complementary
508 sequence to *pUASTattB-LT3-Dam* (Southall et al., 2013) (see Appendix Table S2). Linearised *pUAST-LT3-*
509 *Dam* (digested with NotI and XbaI) was combined with either *MEP-1* or *Mi-2* PCR-amplified coding
510 sequences in a Gibson assembly reaction using NEBuilder® HiFi DNA Assembly kit (NEB) following
511 manufacturers protocols. Resulting N-terminal fusion constructs were injected into *attP2* flies (*y w*
512 *P{y[+t7.7]=nos-phiC31\int.NLS}X #12;; P{y[+t7.7]=CaryP}attP2* – Department of Genetics Microinjection
513 Service, Cambridge) for integration on the third chromosome.

514 *UAS-MTA-1-like-Dam* and *UAS-HDAC1-Dam* were generated using the FlyORF-TaDa cassette exchange
515 protocol as previously described (Aughey et al., 2021). Briefly, *UAS-HDAC1* and *UAS-MTA1-like* FlyORF
516 lines were crossed to *hsFLP; TaDa-FlyORF.* Progeny were heat-shocked at 37 degrees for 45 mins at 96
517 hours following larval hatching. Resulting males were crossed to *Dr/TM6B* and white-eyed F2 males and
518 female virgins used to create a stable stock.

519 **Targeted DamID**

520 Dam fusion or Dam-only males were crossed to virgins of the appropriate driver line for expression of
521 Dam in the desired cell-types. For expression in NBs, all larval neurons (including immature neurons),
522 or mature neurons only - the drivers *wor*-GAL4*; tub*-GAL80^{ts}*, elav*-GAL4*; tub*-GAL80^{ts}*, and nSyb*-GAL4*;*
523 *tub*-GAL80^{ts}, were used, respectively. Embryos were collected for 4 hr then raised at 18°C to prevent
524 premature Dam expression. Animals were transferred to 29°C at 8 days after embryo deposition for 24
525 hours. 60 larval central nervous systems were dissected and stored at -80 degrees. Genomic DNA
526 extraction, methylated DNA enrichment and library preparation were carried out as previously
527 described (Marshall et al., 2016). Two biological replicates were generated for each experiment.

528 Libraries were sequenced with 50 bp single end sequencing on Illumina HiSeq or NovaSeq platforms.
529 >15 million reads were obtained for each library. Data were processed using a previously described Perl
530 pipeline (Marshall and Brand, 2015) (https://github.com/owenjm/damidseq_pipeline).

531 Peak calling was performed using a previously described Perl program (available at
532 https://github.com/tonysouthall/Peak_calling_DamID) which allows for the identification of broadly
533 bound regions that characterise DamID data (Estacio-Gomez et al., 2020). Briefly, false discovery rate
534 (FDR) was calculated for regions consisting of >1 GATC bounded fragments for each replicate.
535 Significant (FDR<0.01%) regions present in all replicates are merged to form a final peak file. Enriched
536 motifs discovery was performed using i-cisTarget on significant peak regions (Herrmann et al., 2012).
537 Intersecting regions for comparison of binding between Mi-2, MEP-1, MTA1-like, or HDAC1 were
538 computed using bedtools intersect utility (Quinlan and Hall, 2010). Similarity between binding peaks
539 was determined using the bedtools jaccard utility, which calculates the ratio between the number of
540 intersecting base pairs and the union between two coordinate sets (Favorov et al., 2012).

541 **Larval crawling assays**

542 Larval crawling assays were conducted as in (Nichols et al., 2012). Briefly, individual third instar
543 wandering larva were placed on room temperature agar with a 10 mm^2 grid placed underneath as a
544 distance reference. Larvae were left to acclimatise for 1 min after which larval movement was tracked
545 visually. Ten animals were used per genotype with three technical replicates performed per animal.

546 **Developmental survival assays**

547 Flies of the appropriate genotype were left in cages containing standard food media supplemented with
548 yeast and left to acclimatise over three nights at 25 °C. Food media was exchanged for apple juice agar
549 and flies left to lay for 5 h. Following the laying period, 100 embryos were transferred to fresh food vials
550 to allow for counting of surviving adults and pupae.

551 **RNA extraction**

552 Three biological replicates were used for knockdown or control samples. Third instar larval CNS were
553 dissected from thirty animals per replicate and total RNA extracted using TRIzol reagent
554 (https://tools.thermofisher.com/content/sfs/manuals/trizol_reagent.pdf) following suppliers
555 protocols. Library preparation and sequencing were subsequently performed by Beijing Genomics
556 Institute (BGI). Sequencing data was mapped to the *Drosophila* genome (release 6.22) using STAR
557 (Dobin et al., 2013). Mapped files were collected in a matrix using featureCounts from the Rsubread
558 package (Liao et al., 2019). Differential expression analysis and MA plots were carried out using the
559 Deseq2 R package (Love et al., 2014).. Genes that had an adjusted p-value <0.05 and a log2 fold change
560 greater than 1 (for upregulated) or less than -1 (for downregulated) were classified as significant.
561 Heatmap generated using pheatmap package in R. Analysis of tissue specific gene enrichment was
562 performed using DGET (Hu et al., 2017).

563 **qRT-PCR**

564 Following RNA extraction, reverse transcription was performed using the iScript cDNA synthesis kit
565 (Bio-Rad), following manufacturer's protocols. qRT-PCR was carried out using iTaq Universal SYBR
566 Green Supermix (Bio-Rad). Expression of target genes was normalised to *Ribosomal Protein L4* (*Rpl4*)
567 and compared to expression in control samples expressing RNAi targeting *mCherry*. Primers amplifying
568 sequences <200 bp were designed to span exon junctions where possible (sequences used can be found
569 in Appendix Table S2. Three biological replicates were carried out for each genotype, with at least two
570 technical replicates for each biological replicate. For each genotype, a Shapiro–Wilks test was performed
571 to calculate if the experimental and control data had normal distributions. If they did, a one-tailed
572 student's t-test was applied, and if not a Welch's t-test was applied.

573

574 **Data availability**

575 All raw sequence files and processed files have been deposited in the National Center for Biotechnology
576 Information Gene Expression Omnibus (GSE199146).

577 **Acknowledgments**

578 We would like to thank the Southall lab and Imperial College fly community for help and feedback on
579 this project. We would like to thank Andrea Brand for generously providing fly stocks and the Dpn
580 antibody. We also thank the Bloomington *Drosophila* Stock Center (NIH P40OD018537) for fly stocks.
581 This work was funded by a Wellcome Trust Investigator grant 104567 to T.D.S and a BBSRC grant
582 BB/P017924/1 to T.D.S. and G.N.A.

583 **Disclosure and competing interests statement**

584 The authors have no conflicts of interest to disclose.

585 **References**

586 Amaya, M., Desai, M., Gnanapragasam, M.N., Wang, S.Z., Zu Zhu, S., Williams, D.C., Jr., and Ginder, G.D.
587 (2013). Mi2beta-mediated silencing of the fetal gamma-globin gene in adult erythroid cells. *Blood* 121,
588 3493-3501.

589 Arends, T., Dege, C., Bortnick, A., Danhorn, T., Knapp, J.R., Jia, H., Harmacek, L., Fleenor, C.J., Straign, D.,
590 Walton, K., *et al.* (2019). CHD4 is essential for transcriptional repression and lineage progression in B
591 lymphopoiesis. *Proc Natl Acad Sci U S A* 116, 10927-10936.

592 Aughey, G.N., Delandre, C., McMullen, J.P.D., Southall, T.D., and Marshall, O.J. (2021). FlyORF-TaDa allows
593 rapid generation of new lines for in vivo cell-type-specific profiling of protein-DNA interactions in
594 Drosophila melanogaster. *G3 (Bethesda)* 11.

595 Aughey, G.N., Estacio Gomez, A., Thomson, J., Yin, H., and Southall, T.D. (2018). CATaDa reveals global
596 remodelling of chromatin accessibility during stem cell differentiation in vivo. *Elife* 7.

Bagni, C., Bray, S., Gogos, J.A., Kafatos, F.C., and Hsu, T. (2002). The Drosophila zinc finger transcription factor CF2 is a myogenic marker downstream of MEF2 during muscle development. *Mech Dev* 117, 265-268.

Berger, C., Renner, S., Luer, K., and Technau, G.M. (2007). The commonly used marker ELAV is transiently expressed in neuroblasts and glial cells in the Drosophila embryonic CNS. *Dev Dyn* 236, 3562-3568.

Bolte, S., and Cordelieres, F.P. (2006). A guided tour into subcellular colocalization analysis in light microscopy. *J Microsc* 224, 213-232.

Bornelov, S., Reynolds, N., Xenophontos, M., Gharbi, S., Johnstone, E., Floyd, R., Ralser, M., Signolet, J., Loos, R., Dietmann, S.*, et al.* (2018). The Nucleosome Remodeling and Deacetylation Complex Modulates Chromatin Structure at Sites of Active Transcription to Fine-Tune Gene Expression. *Mol Cell* 71, 56-72 e54.

Brehm, A., Langst, G., Kehle, J., Clapier, C.R., Imhof, A., Eberharter, A., Muller, J., and Becker, P.B. (2000). dMi-2 and ISWI chromatin remodelling factors have distinct nucleosome binding and mobilization properties. *EMBO J* 19, 4332-4341.

Burgold, T., Barber, M., Kloet, S., Cramard, J., Gharbi, S., Floyd, R., Kinoshita, M., Ralser, M., Vermeulen, M., Reynolds, N.*, et al.* (2019). The Nucleosome Remodelling and Deacetylation complex suppresses transcriptional noise during lineage commitment. *EMBO J* 38.

Dobin, A., Davis, C.A., Schlesinger, F., Drenkow, J., Zaleski, C., Jha, S., Batut, P., Chaisson, M., and Gingeras, T.R. (2013). STAR: ultrafast universal RNA-seq aligner. *Bioinformatics* 29, 15-21.

Eichler, K., Li, F., Litwin-Kumar, A., Park, Y., Andrade, I., Schneider-Mizell, C.M., Saumweber, T., Huser, A., Eschbach, C., Gerber, B.*, et al.* (2017). The complete connectome of a learning and memory centre in an insect brain. *Nature* 548, 175-182.

Estacio-Gomez, A., Hassan, A., Walmsley, E., Le, L.W., and Southall, T.D. (2020). Dynamic neurotransmitter specific transcription factor expression profiles during Drosophila development. *Biol Open* 9.

Favorov, A., Mularoni, L., Cope, L.M., Medvedeva, Y., Mironov, A.A., Makeev, V.J., and Wheelan, S.J. (2012). Exploring massive, genome scale datasets with the GenometriCorr package. *PLoS Comput Biol* 8, e1002529.

Filion, G.J., van Bemmel, J.G., Braunschweig, U., Talhout, W., Kind, J., Ward, L.D., Brugman, W., de Castro, I.J., Kerkhoven, R.M., Bussemaker, H.J.*, et al.* (2010). Systematic protein location mapping reveals five principal chromatin types in Drosophila cells. *Cell* 143, 212-224.

Gomez-Del Arco, P., Perdiguero, E., Yunes-Leites, P.S., Acin-Perez, R., Zeini, M., Garcia-Gomez, A., Sreenivasan, K., Jimenez-Alcazar, M., Segales, J., Lopez-Maderuelo, D.*, et al.* (2016). The Chromatin Remodeling Complex Chd4/NuRD Controls Striated Muscle Identity and Metabolic Homeostasis. *Cell Metab* 23, 881-892.

Hassan, A., Araguas Rodriguez, P., Heidmann, S.K., Walmsley, E.L., Aughey, G.N., and Southall, T.D. (2020). Condensin I subunit Cap-G is essential for proper gene expression during the maturation of post-mitotic neurons. *Elife* 9.

Herrmann, C., Van de Sande, B., Potier, D., and Aerts, S. (2012). i-cisTarget: an integrative genomics method for the prediction of regulatory features and cis-regulatory modules. *Nucleic Acids Res* 40, e114.

Ho, J.W., Jung, Y.L., Liu, T., Alver, B.H., Lee, S., Ikegami, K., Sohn, K.A., Minoda, A., Tolstorukov, M.Y., Appert, A.*, et al.* (2014). Comparative analysis of metazoan chromatin organization. *Nature* 512, 449-452.

Hoffmann, A., and Spengler, D. (2019). Chromatin Remodeling Complex NuRD in Neurodevelopment and Neurodevelopmental Disorders. *Front Genet* 10, 682.

641 Hsu, T., Bagni, C., Sutherland, J.D., and Kafatos, F.C. (1996). The transcriptional factor CF2 is a mediator
642 of EGF-R-activated dorsoventral patterning in Drosophila oogenesis. *Genes Dev* 10, 1411-1421.

643 Hu, Y., Comjean, A., Perrimon, N., and Mohr, S.E. (2017). The Drosophila Gene Expression Tool (DGET)
644 for expression analyses. *BMC Bioinformatics* 18, 98.

645 Huang, Z., and Kunes, S. (1996). Hedgehog, transmitted along retinal axons, triggers neurogenesis in the
646 developing visual centers of the Drosophila brain. *Cell* 86, 411-422.

647 Janssens, J., Aibar, S., Taskiran, II, Ismail, J.N., Gomez, A.E., Aughey, G., Spanier, K.I., De Rop, F.V., Gonzalez-
648 Blas, C.B., Dionne, M.*, et al.* (2022). Decoding gene regulation in the fly brain. *Nature*.

649 Jiao, W., Spreemann, G., Ruchti, E., Banerjee, S., Shi, Y., Stowers, R.S., Hess, K., and McCabe, B.D. (2021).
650 Intact Drosophila Whole Brain Cellular Quantitation reveals Sexual Dimorphism. *bioRxiv*,
651 2021.2011.2003.467146.

652 Johnson, P.W., Doe, C.Q., and Lai, S.L. (2018). Drosophila nucleostemin 3 is required to maintain larval
653 neuroblast proliferation. *Dev Biol* 440, 1-12.

654 Krause, S.A., Overend, G., Dow, J.A.T., and Leader, D.P. (2022). FlyAtlas 2 in 2022: enhancements to the
655 Drosophila melanogaster expression atlas. *Nucleic Acids Res* 50, D1010-D1015.

656 Kreher, J., Kovac, K., Bouazoune, K., Macinkovic, I., Ernst, A.L., Engelen, E., Pahl, R., Finkernagel, F.,
657 Murawska, M., Ullah, I.*, et al.* (2017). EcR recruits dMi-2 and increases efficiency of dMi-2-mediated
658 remodelling to constrain transcription of hormone-regulated genes. *Nat Commun* 8, 14806.

659 Kunert, N., Wagner, E., Murawska, M., Klinker, H., Kremmer, E., and Brehm, A. (2009). dMec: a novel Mi-
660 2 chromatin remodelling complex involved in transcriptional repression. *EMBO J* 28, 533-544.

661 Lattao, R., Kovacs, L., and Glover, D.M. (2017). The Centrioles, Centrosomes, Basal Bodies, and Cilia of
662 Drosophila melanogaster. *Genetics* 206, 33-53.

663 Liao, Y., Smyth, G.K., and Shi, W. (2019). The R package Rsubread is easier, faster, cheaper and better for
664 alignment and quantification of RNA sequencing reads. *Nucleic Acids Res* 47, e47.

665 Love, M.I., Huber, W., and Anders, S. (2014). Moderated estimation of fold change and dispersion for
666 RNA-seq data with DESeq2. *Genome Biol* 15, 550.

667 Low, J.K., Webb, S.R., Silva, A.P., Saathoff, H., Ryan, D.P., Torrado, M., Brofelth, M., Parker, B.L., Shepherd,
668 N.E., and Mackay, J.P. (2016). CHD4 Is a Peripheral Component of the Nucleosome Remodeling and
669 Deacetylase Complex. *J Biol Chem* 291, 15853-15866.

670 Marshall, O.J., and Brand, A.H. (2015). damidseq_pipeline: an automated pipeline for processing DamID
671 sequencing datasets. *Bioinformatics* 31, 3371-3373.

672 Marshall, O.J., and Brand, A.H. (2017). Chromatin state changes during neural development revealed by
673 in vivo cell-type specific profiling. *Nat Commun* 8, 2271.

674 Marshall, O.J., Southall, T.D., Cheetham, S.W., and Brand, A.H. (2016). Cell-type-specific profiling of
675 protein-DNA interactions without cell isolation using targeted DamID with next-generation sequencing.
676 *Nat Protoc* 11, 1586-1598.

677 Nichols, C.D., Becnel, J., and Pandey, U.B. (2012). Methods to assay Drosophila behavior. *J Vis Exp*.

678 Nitarska, J., Smith, J.G., Sherlock, W.T., Hillege, M.M., Nott, A., Barshop, W.D., Vashisht, A.A., Wohlschlegel,
679 J.A., Mitter, R., and Riccio, A. (2016). A Functional Switch of NuRD Chromatin Remodeling Complex
680 Subunits Regulates Mouse Cortical Development. *Cell Rep* 17, 1683-1698.

681 O'Shaughnessy-Kirwan, A., Signolet, J., Costello, I., Gharbi, S., and Hendrich, B. (2015). Constraint of gene
682 expression by the chromatin remodelling protein CHD4 facilitates lineage specification. *Development*
683 142, 2586-2597.

684 Preissl, S., Fang, R., Huang, H., Zhao, Y., Raviram, R., Gorkin, D.U., Zhang, Y., Sos, B.C., Afzal, V., Dickel, D.E.,
685 *et al.* (2018). Single-nucleus analysis of accessible chromatin in developing mouse forebrain reveals cell-
686 type-specific transcriptional regulation. *Nat Neurosci* 21, 432-439.

687 Quinlan, A.R., and Hall, I.M. (2010). BEDTools: a flexible suite of utilities for comparing genomic features.
688 *Bioinformatics* 26, 841-842.

689 Ragheb, R., Gharbi, S., Cramard, J., Ogundele, O., Kloet, S.L., Burgold, T., Vermeulen, M., Reynolds, N., and
690 Hendrich, B. (2020). Differential regulation of lineage commitment in human and mouse primed
691 pluripotent stem cells by the nucleosome remodelling and deacetylation complex. *Stem Cell Res* 46,
692 101867.

693 Rais, Y., Zviran, A., Geula, S., Gafni, O., Chomsky, E., Viukov, S., Mansour, A.A., Caspi, I., Krupalnik, V.,
694 Zerbib, M., *et al.* (2013). Deterministic direct reprogramming of somatic cells to pluripotency. *Nature*
695 502, 65-70.

696 Ravenscroft, T.A., Janssens, J., Lee, P.T., Tepe, B., Marcogliese, P.C., Makhzami, S., Holmes, T.C., Aerts, S.,
697 and Bellen, H.J. (2020). Drosophila Voltage-Gated Sodium Channels Are Only Expressed in Active
698 Neurons and Are Localized to Distal Axonal Initial Segment-like Domains. *J Neurosci* 40, 7999-8024.

699 Reddington, J.P., Garfield, D.A., Sigalova, O.M., Karabacak Calviello, A., Marco-Ferreres, R., Girardot, C.,
700 Viales, R.R., Degner, J.F., Ohler, U., and Furlong, E.E.M. (2020). Lineage-Resolved Enhancer and Promoter
701 Usage during a Time Course of Embryogenesis. *Dev Cell* 55, 648-664 e649.

702 Reddy, B.A., Bajpe, P.K., Bassett, A., Moshkin, Y.M., Kozhevnikova, E., Bezstarosti, K., Demmers, J.A.,
703 Travers, A.A., and Verrijzer, C.P. (2010). Drosophila transcription factor Tramtrack69 binds MEP1 to
704 recruit the chromatin remodeler NuRD. *Mol Cell Biol* 30, 5234-5244.

705 Rhee, D.Y., Cho, D.Y., Zhai, B., Slattery, M., Ma, L., Mintseris, J., Wong, C.Y., White, K.P., Celniker, S.E.,
706 Przytycka, T.M., *et al.* (2014). Transcription factor networks in Drosophila melanogaster. *Cell Rep* 8,
707 2031-2043.

708 Selleck, S.B., and Steller, H. (1991). The influence of retinal innervation on neurogenesis in the first optic
709 ganglion of Drosophila. *Neuron* 6, 83-99.

710 Southall, T.D., Davidson, C.M., Miller, C., Carr, A., and Brand, A.H. (2014). Dedifferentiation of neurons
711 precedes tumor formation in Lola mutants. *Dev Cell* 28, 685-696.

712 Southall, T.D., Gold, K.S., Egger, B., Davidson, C.M., Caygill, E.E., Marshall, O.J., and Brand, A.H. (2013). Cell-
713 type-specific profiling of gene expression and chromatin binding without cell isolation: assaying RNA
714 Pol II occupancy in neural stem cells. *Dev Cell* 26, 101-112.

715 Tie, F., Furuyama, T., Prasad-Sinha, J., Jane, E., and Harte, P.J. (2001). The Drosophila Polycomb Group
716 proteins ESC and E(Z) are present in a complex containing the histone-binding protein p55 and the
717 histone deacetylase RPD3. *Development* 128, 275-286.

718 Tong, J.K., Hassig, C.A., Schnitzler, G.R., Kingston, R.E., and Schreiber, S.L. (1998). Chromatin
719 deacetylation by an ATP-dependent nucleosome remodelling complex. *Nature* 395, 917-921.

720 Unhavaithaya, Y., Shin, T.H., Miliaras, N., Lee, J., Oyama, T., and Mello, C.C. (2002). MEP-1 and a homolog
721 of the NURD complex component Mi-2 act together to maintain germline-soma distinctions in C. elegans.
722 *Cell* 111, 991-1002.

723 Wade, P.A., Jones, P.L., Vermaak, D., and Wolffe, A.P. (1998). A multiple subunit Mi-2 histone deacetylase
724 from Xenopus laevis cofractionates with an associated Snf2 superfamily ATPase. *Curr Biol* 8, 843-846.

725 Wang, H.B., and Zhang, Y. (2001). Mi2, an auto-antigen for dermatomyositis, is an ATP-dependent
726 nucleosome remodeling factor. *Nucleic Acids Res* 29, 2517-2521.

Wang, Z., Zang, C., Cui, K., Schones, D.E., Barski, A., Peng, W., and Zhao, K. (2009). Genome-wide mapping of HATs and HDACs reveals distinct functions in active and inactive genes. *Cell* 138, 1019-1031.

Xue, Y., Wong, J., Moreno, G.T., Young, M.K., Cote, J., and Wang, W. (1998). NURD, a novel complex with both ATP-dependent chromatin-remodeling and histone deacetylase activities. *Mol Cell* 2, 851-861.

Yamada, T., Yang, Y., Hemberg, M., Yoshida, T., Cho, H.Y., Murphy, J.P., Fioravante, D., Regehr, W.G., Gygi, S.P., Georgopoulos, K.*, et al.* (2014). Promoter decommissioning by the NuRD chromatin remodeling complex triggers synaptic connectivity in the mammalian brain. *Neuron* 83, 122-134.

Yoshida, T., Hazan, I., Zhang, J., Ng, S.Y., Naito, T., Snippert, H.J., Heller, E.J., Qi, X., Lawton, L.N., Williams, C.J.*, et al.* (2008). The role of the chromatin remodeler Mi-2beta in hematopoietic stem cell self-renewal and multilineage differentiation. *Genes Dev* 22, 1174-1189.

Zacharioudaki, E., Falo Sanjuan, J., and Bray, S. (2019). Mi-2/NuRD complex protects stem cell progeny from mitogenic Notch signaling. *Elife* 8.

Zhang, W., Aubert, A., Gomez de Segura, J.M., Karuppasamy, M., Basu, S., Murthy, A.S., Diamante, A., Drury, T.A., Balmer, J., Cramard, J.*, et al.* (2016). The Nucleosome Remodeling and Deacetylase Complex NuRD Is Built from Preformed Catalytically Active Sub-modules. *J Mol Biol* 428, 2931-2942.

Zhang, Y., LeRoy, G., Seelig, H.P., Lane, W.S., and Reinberg, D. (1998). The dermatomyositis-specific autoantigen Mi2 is a component of a complex containing histone deacetylase and nucleosome remodeling activities. *Cell* 95, 279-289.

Ziffra, R.S., Kim, C.N., Ross, J.M., Wilfert, A., Turner, T.N., Haeussler, M., Casella, A.M., Przytycki, P.F., Keough, K.C., Shin, D.*, et al.* (2021). Single-cell epigenomics reveals mechanisms of human cortical development. *Nature* 598, 205-213.

Figure Legends

Figure 1. Critical role of *Mi-2* RNAi in *Drosophila* neurons. A) Third instar larval CNS of *Mi-2* GFP-trap line (scale bar = 20 μm). White arrows highlight NSC nuclei. B) Survival of *Mi-2* RNAi and control (*mCherry-RNAi*) flies during development (**** $p < 0.001$).* D) Larval crawl speed (cm/minute) in *Mi-2* RNAi and *mCherry* RNAi controls (** $p < 0.01$).

Figure 2. Genomic binding of NuRD components. A) Principal component analysis of all NuRD component binding in neurons including replicates. Mi-2/MEP-1 (blue/purple) cluster independently of MTA1-like (green) and HDAC1 (orange) reflecting greater similarity in their binding profiles. B) Heatmap and enrichment plots indicating binding at Mi-2 peaks. C) Venn diagrams indicating the number of overlapping peaks between NuRD subunits. All intersections between peaks occur at statistically significant frequencies (Fisher's exact test $p < 10^{-24}$). D) Peak annotation for Mi-2, MEP-1, MTA-1like and HDAC1 peaks. E) Top enriched motifs at NuRD and dMec peaks. F) Heatmap indicating jaccard similarity statistic between chromatin states and NuRD peaks (Mi-2, MEP-1, MTA-1like and HDAC1) and dMEC (Mi-2 and MEP-1 only), or HDAC1 peaks.

Figure 3. *Mi-2* knockdown in larval neurons results in extensive gene expression changes. A) Volcano plot showing significantly up-regulated (green) and down-regulated (purple) genes with fold-change. Selected mis-expressed genes are annotated. B) RNA-seq tracks showing *vas* mRNA expression

766 in third instar larval CNS (Y-axis is RPKM). C) Heatmap showing relative changes in normalised read-
767 counts between *Mi-2* RNAi and control replicates for all significantly differentially expressed genes (p-
768 adj < 0.05, log2 fold change >1 or <-1). Significantly more genes are upregulated (1467) than
769 downregulated (397). D) Enriched gene ontology terms for genes that are upregulated in *Mi-2* RNAi
770 knockdown. E) Heatmap showing relative expression levels of upregulated genes across selected
771 *Drosophila* tissues (full version in Appendix Figure S2).

772 **Figure 4. *dMec* knockdown causes ectopic gene expression and *NuRD* knockdown in neurons**
773 **causes an optic lobe development phenotype.**
774 A) Quantification of candidate gene expression (selected from upregulated genes in RNA-seq data) in
775 knockdown genotypes (3 biological replicates for each group). ** *p < 0.01 and *** p < 0.001* (one-tailed
776 student's t-test or Welch's t-test against control) Represented as mean ± SEM. B) Quantification of
777 optic lobe neuroepithelial cells of genotypes shown in panel C (n >= 9 for each group). *** *p < 0.001*
778 (one-tailed student's t-test or Welch's t-test against control). Represented as a box plot. C)
779 Representative images of control (*elav*-GAL4*; ; mCherry*^{RNAi}), *Mi-2* knockdown, *MEP-1* knockdown,
780 *HDAC1* knockdown and *MBD-like* knockdown in the third instar larval CNS (all scale bars = 20 µm).
781 Discs large (Dlg) = green, Deadpan (Dpn) = magenta. Neuroepithelial cells are highlighted by dashed
782 lines.
783

784 **Figure 5. Differential requirements of Mi-2 during neuronal differentiation.** A) Ectopic
785 expression of *vas* when *Mi-2* is knocked down at different stages of differentiation. (3 biological
786 replicates for each group). * *p < 0.05* and ** *p < 0.01* (one-tailed student's t-test against control)
787 Represented as mean ± SEM. B) Representation of expression of GAL4 drivers used. C) Larval brain
788 optic lobe morphology when *Mi-2* is knocked down at different stages of differentiation Elav = green,
789 Dpn = magenta.

790 **Figure 6. Dynamic Mi-2 binding during neuronal differentiation.** A) Examples of differential
791 genomic binding of Mi-2 at neural genes. B) Overlap of Mi-2 binding peaks in NSCs, immature neurons
792 and mature neurons. C) Number and overlap of genes with differential Mi-2 binding. D) Motif analysis
793 of differentially bound regions.

794

795